HOMO Stabilisation in π-Extended Dibenzotetrathiafulvalene Derivatives for Their Application in OFETs

Yan Geng,[a] Raphael Pfattner,[b] Antonio Campos,[b] Wei Wang, [a,c] Olivier Jeannin,[a,d] Jürg Hauser,[a] Joaquim Puigdollers,[e] Stefan T. Bromley,[f] Silvio Decurtins,[a] Jaume Veciana,[b] Concepció Rovira,[b] Marta Mas-Torrent*[b] and Shi-Xia Liu*[a]

Abstract: Three new organic semiconductors, where either two methoxy units are directly linked to the dibenzotetrathiafulvalene (DB-TTF) central core and a 2,1,3-chalcogendiazole is fused on the one side or four methoxy groups are linked to the DB-TTF, have been synthesised as active materials for organic field-effect transistors (OFETs). Their electrochemical behaviour, electronic absorption and fluorescence emission as well as photoinduced intramolecular charge transfer were studied. The electron-withdrawing 2,1,3-chalcogendiazole unit significantly affects the electronic properties of these semiconductors, lowering the HOMO and LUMO energy levels and hence increasing the stability of the semiconducting material. The solution-processed single crystal transistors exhibit high performance with a hole mobility up to 0.04 $cm^2 V^{-1} s^{-1}$ as well as good ambient stability.

Keywords: tetrathiafulvalene • donor-acceptor systems • organic field effect transistors • ring-fused systems • molecular electronics

Introduction

Organic field-effect transistors (OFETs) are of intensive scientific and technological interest due to their appealing electronic applications, for instance low-cost integrated circuits and flexible displays.[1] Over the past two decades, a vast number of organic semiconductors including acene, rubrene and tetrathiafulvalene (TTF) molecules have been reported as active materials in OFETs.[2] In particular, solution-processed single crystal transistors based on dibenzotetrathiafulvalene (DB-TTF) show excellent OFET performances with a high mobility on the order of 0.1-1 $cm^2/V{\cdot}s$, although thin films of this material become easily doped in air.[3] Consequently, a few alkyl substituted, fluorinated, phthalimide- or pyrazine-fused DB-TTF derivatives were investigated to explore the relationship between structures and OFET characteristics such as charge carrier mobility, on/off ratio, threshold voltage as well as ambient stability.[4] Here, with the aim of gaining environmental stability, electron-deficient nitrogen heterocycles such as 2,1,3-chalcogendiazole and electron-rich methoxy groups have been considered to directly fuse into the DB-TTF skeleton (Compounds **1-3**, Figure 1). Recently, 2,1,3-benzothiadiazole[5-7] has become a key ingredient in the design of new organic semiconductors and it is often embedded in simple conjugated structures or polymers, whereby its electron-deficient character serves to stabilize and spatially localize the lowest-unoccupied molecular orbital (LUMO), hence it functions as an E_{LUMO} lowering π-extender. On the one hand, an enhanced stability to oxygen can be achieved by the direct fusion of the 2,1,3-chalcogendiazole moiety to the DB-TTF core due to the lowering of the HOMO levels.[8] Moreover, rigid donor-acceptor (D-A) ensembles such as **2** and **3** can impart a strong dipole-dipole interaction leading to enhanced intermolecular π–π interactions and a large transfer integral between molecules.[9] Such factors are crucial for achieving high carrier mobility. For a comparative and systematic study, tetramethoxy substituted DB-TTF (**1**) is also presented. In the present work, we have reported synthesis, characterization and electronic properties of compounds 1-3 (Figure 1) and explored their application in OFETs..

[a] Dr. Yan Geng, Prof. Wei Wang, Dr. Olivier Jeannin, Dr. Jürg Hauser, Prof. Silvio Decurtins, Dr. Shi-Xia Liu
Departement für Chemie und Biochemie
Universität Bern
Freiestrasse 3, 3012 Bern, Schweiz
Fax: (+) 41 31 631 4399
E-mail: liu@dcb.unibe.ch

[b] Dr. Raphael Pfattner, Antonio Campos, Prof. Jaume Veciana, Prof. Concepció Rovira, Dr. Marta Mas-Torrent
Institut de Ciència de Materials de Barcelona (ICMAB-CSIC) and Networking Research Center on Bioengineering
Biomaterials and Nanomedicine (CIBER-BBN)
Campus UAB
08193 Bellaterra, Spain
Fax: (+) 34 935 805 729
E-mail: mmas@icmab.es

[c] Prof. Wei Wang
Present address: Key Laboratory of Sensor Analysis of Tumor Marker
Ministry of Education, College of Chemistry and Molecular Engineering
Qingdao University of Science and Technology
Qingdao 266042, P. R. China.

[d] Dr. Olivier Jeannin
Present address: Université de Rennes 1-UMR CNRS 6226
"Sciences Chimiques de Rennes"-MaCSE group. Bat 10C
Campus de Beaulieu - 35042 Rennes cedex, France.

[e] Dr. Joaquim Puigdollers
Dept. Enginyeria Electrònica
Universitat Politècnica Catalunya
08034 Barcelona, Spain

[f] Prof. Stefan T. Bromley
Departament de Química Física & Institut de Química Teòrica i Computacional (IQTCUB), Universitat de Barcelona
08028 Barcelona, Spain, and Institució Catalana de Recerca i Estudis Avançats (ICREA), 08010 Barcelona, Spain

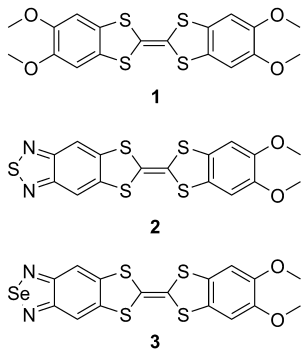

Figure 1. Chemical structures of three new TTF-based semiconductors.

Results and Discussion

Synthesis: The synthetic pathway to prepare **1-3** is outlined in Scheme 1. The target compound **1** was prepared by a phosphite-mediated homo-coupling reaction of the corresponding ketone precursor **5**. The preparation of **5** is accomplished by a reaction of 4,5-bis-thiobutylveratrole[10] with CS_2 followed by oxidation in the presence of $Hg(OAc)_2$. The formation of the compound **4** involved the well-known cleavage of the C-S bond in liquid ammonia by alkali metals[11] to afford an intermediate disodium salt of 1,2-dithio-4,5-dimethoxybenzene that can easily react with CS_2. The target compounds **2** and **3** were obtained by a phosphite-mediated cross-coupling reaction of the corresponding thione precursor **6**[12] or **7**[13] with ketone **5**. All new compounds were purified by chromatographic separation and/or recrystallisation. Their identity was established by NMR, HRMS data and elemental analysis.

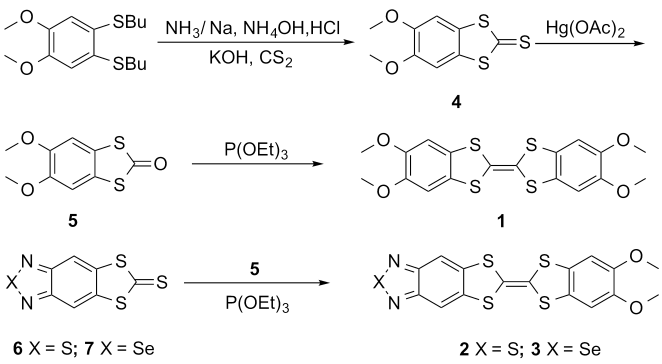

Scheme 1. Synthetic routes to targets **1-3**.

Electrochemistry: The oxidation potentials of **1-3** were measured by cyclic voltammetry using a Pt wire as a counter and working electrode and a silver wire as a pseudo-reference electrode (Table 1 and Figure S1). Ferrocene/Ferrocenium (Fc/Fc^+) was used as internal reference, showing an oxidation potential of 0.44 V *vs* Ag(s) in the experimental conditions employed (see experimental section). The three compounds show two oxidation waves attributed to the formation of the TTF radical cation and dication species. The fusion of the electron-withdrawing 2,1,3-benzochalcogendiazole (BCD) unit leads to a positive shift of the oxidation potentials, thus increasing the stability to oxygen. Under the premise that the energy level of ferrocene/ferrocenium is 4.8 eV below the vacuum level,[14] the the highest-occupied molecular orbital (HOMO) energy levels of **1-3** can be estimated according to: $E_{HOMO} = -[E_{onset}^{ox1} + 4.8]$ (eV), where E_{onset}^{ox1} is the onset oxidation potential of the first redox wave versus Fc/Fc^+.[15] For the three molecules the HOMO levels were found in the range -4.5 to -4.8 eV. No reduction processes were observed under the used conditions for any of the molecules down to -1.5 V vs Ag(s).

Optical properties and DFT calculations of the energy levels: The optical absorption spectra of **1-3** in THF solution are shown in Figure 2. All these compounds exhibit intense absorption bands at $\lambda < 400$ nm with extinction coefficients on the order of 2×10^4 $M^{-1}cm^{-1}$. Additionally, compounds **2** and **3** show an intense absorption band peaking at 485 nm and 511 nm, respectively, which is absent for compound **1**. According to our previous observations,[6,12,13] this lowest energy absorption band corresponds to an intramolecular charge-transfer transition from the HOMO localized on the TTF core to the LUMO localized on the BCD moiety, as depicted in Figure 3. Moreover, both compounds, **2** and **3**, are emissive with an emission maximum at 652 nm and 695 nm, respectively. Therefore, the optical HOMO-LUMO energy gaps of **2** and **3** can be determined from the intersection of the absorption and emission spectra in THF. The obtained E_g^{opt} values are in good agreement with the corresponding E_g^{calc} (see below) values (Table 1). It is worthwhile to note that band gaps can be tuned by the incorporation of different substituents into the DB-TTF structures as well as by the variation of the heteroatom in the 2,1,3-chalcogendiazole moiety.

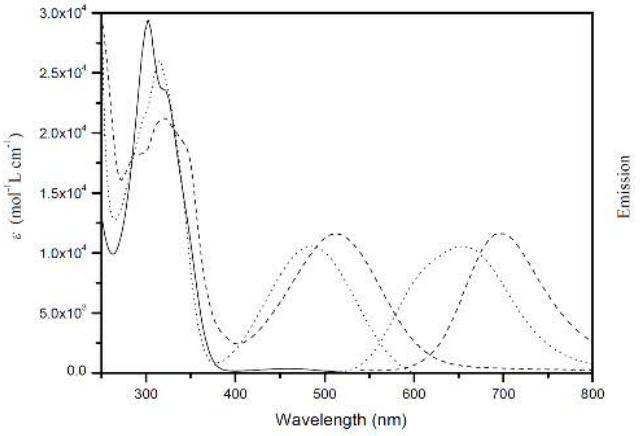

Figure 2. Optical absorption and emission spectra of **1** (solid line), **2** (dotted line) and **3** (dashed line) in THF at room temperature.

Density functional theory (DFT) calculations were performed for **1-3** using the B3LYP functional[16] and a 6-311G+(d, p) basis set as implemented in the Gaussian 09 code.[17] All of the investigated molecules have a quite planar molecular skeleton, beneficial for intermolecular interactions, which favours charge-carrier mobility. Compared to **1**, it is clear that **2** and **3** possess relatively lower-lying HOMO and LUMO levels upon replacing dimethoxy groups with the 2,1,3-chalcogendiazole unit. Exchanging sulfur by selenium appears to slightly decrease the LUMO energy level further. The match between the relative magnitudes and absolute quantitative values of the calculated HOMO energy levels and HOMO-LUMO gaps and the corresponding experimental HOMO values and energy gap values obtained from cyclic voltammetry and absorption spectral data, respectively, is in nearly all cases rather good. The small differences between experiment and theory (typically ≤ 0.3 eV) are quite acceptable especially considering the approximations in the theoretical calculations (e.g. absence of explicit solvent

effects and intermolecular interactions). As expected, in all cases the HOMO is localised on the TTF core, while the LUMO is mainly located on the 2,1,3-chalcogendiazole unit in compounds **2** and **3** and on the TTF core in compound **1** (see Figure 3).

Table 1. Redox Potentials (*V versus* Fc/Fc^+), lowest energy absorption and emission maxima, A_{max} and E_{max} respectively, extinction coefficient ε, Stokes shift ν_{ST}, optical band gap E_g^{opt} as well as the calculated HOMO and LUMO energies (E_{HOMO} and E_{LUMO}) and HOMO-LUMO gaps E_g^{calc} of compounds **1-3**.

Compound		1	2	3
Electrochemical data	$E_{1/2}^{ox1}$	-0.29[b]	-0.01.[a]	0.11[a]
	$E_{1/2}^{ox2}$	0.25[b]	-0.46[a]	0.59[a]
	E_{onset}^{ox1}	-0.34	-0.11	0.02
	E_{HOMO} [eV][c]	-4.5	-4.7	-4.8
UV-Vis and emission spectral data	A_{max} [cm^{-1}]	33110	20620	19570
	ε [$M^{-1}cm^{-1}$]	2.81×10^4	1.06×10^4	1.16×10^4
	E_{max} [cm^{-1}]	-	15337	14388
	ν_{ST} [cm^{-1}]	-	5283	5182
	E_g^{opt} [eV]	3.26[d]	2.21[e]	2.01[e]
DFT calculations	E_{HOMO}[eV]	-4.46	-5.08	-5.08
	E_{LUMO}[eV]	-1.14	-2.70	-2.79
	E_g^{calc} [eV]	3.32	2.38	2.29

[a] reversible peak. [b] quasi-reversible peak. [c] estimated from the onset oxidation potentials using empirical equations: $E_{HOMO} = -[E_{onset}^{ox1} + 4.8]$eV. [d] determined from the onset of the lowest energy electronic absorption in the UV-vis spectrum in THF. [e] determined from the intersection of the absorption and emission spectra in THF.

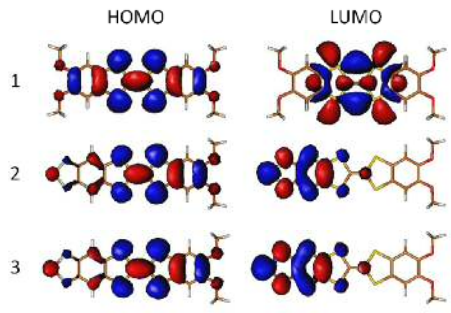

Figure 3. HOMO and LUMO orbitals of molecules **1-3**.

Crystal structure of 1: Orange coloured single crystals for X-ray analysis, with a block-shaped morphology, were grown by slow evaporation of a CH_2Cl_2/hexane (1:1) solution of **1**. The compound crystallises in a solvate free form in the monoclinic space group $P2_1/c$. The molecule lies on an inversion centre, therefore the asymmetric unit comprises half of the molecule. An ORTEP drawing of **1** is shown in Figure 4a. The molecule is distinctly planar; the rms deviation from a least-squares plane through all atoms (excluding the hydrogen atoms) is only 0.049 Å, and for the TTF core alone it is 0.017 Å. In the crystal structure, adjacent molecules are arranged in a nearly orthogonal manner forming an herringbone packing (Figure 4b, and Figure S2-S3). Close S···S intermolecular contacts of 3.758 Å in the *bc* plane are found, and also there are some short C···S contacts of 3.375 Å and 3.468 Å and weak O···H interactions with distances of 2.510 Å.

Dimers of **1** taken from the experimental crystal structure were used to calculate the hole transfer integrals, t_h. Following ref [18], DFT calculations using the PW91 functional[19] and a 6-31G(d,p) basis set were employed for calculating the HOMO energy splitting in the dimers (where the t_h are taken to be half of the HOMO splitting energies). This parameter gives information about the strength of the interactions between the HOMO electronic levels of the molecules involved in the charge-transfer process. Considering the crystal structure, three close pairs of neighbouring molecules were considered (two of them are indicated in Figure 4b). A large transfer integral was found in the d_1 direction (224.0 meV) and also a significant value along the edge-to-face d_2 direction (56.2 meV). However, almost negligible electronic interactions (0.1 meV) can be found between neighbouring molecules along the *a* axis. Similar intermolecular interactions in TTFs have been shown to be efficient for leading to high electronic intermolecular overlap and high charge carrier field-effect mobility.[2a,20]

Organic field-effect transistors: Solution grown single crystal OFETs were fabricated with compounds **1-3** by drop casting on Si/SiO_2 substrates a solution of the molecules in 1,2-dichlorobenzene at a concentration of c = 0.5 mg/ml at T = 100°C for compounds **1-2,** and at room temperature for compound **3**. In all cases, elongated plate-like crystals were obtained. Afterwards graphite source and drain electrodes were painted on top of single crystals of **1** and **2**, while for **3** prefabricated Cr/Au electrodes were used as source and drain. The OFET characteristics of a typical single crystal based on **1**, measured under ambient conditions and in darkness, are illustrated in Figure 5. This OFET based on **1** shows typical electrical *p*-channel characteristics. The channel dimensions were measured with the optical microscope and found to be W = 170 µm, L = 550 µm. A negligible hysteresis was observed between forward and reverse V_D sweeps. Furthermore, a low threshold voltage of about V_{TH} = -1.1 V was extracted in the saturation regime, indicating a low level of unintentional doping of the active material. From the saturation regime a field-effect mobility of μ_{FE} = 0.020 ± 0.003 cm^2/Vs was extracted. This mobility is of the same order of other solution processed TTF OFETs.[4b,21] A set of 4 devices was measured exhibiting similar values in terms of device performance and OFET characteristics. Single crystal OFETs based on compounds **2** and **3** exhibited good performance with typical field effect mobilities in the saturation regime of about μ_{FE} = 0.014 ± 0.005 cm^2/Vs and μ_{FE} = 0.04 ± 0.02 cm^2/Vs, respectively (Figure S4 and S5). The threshold voltages were found to be V_{TH} = -4 V and V_{TH} = -0.3 V, for **2** and **3**, respectively. These values are considered to be quite low in OFETs and point towards a favourable organic/dielectric interface with a very modest number of charge trapping sites and undoped organic semiconductors. All these device data parameters are collected in Table 2. It should be highlighted that all the devices turned out to be stable in air for over a week.

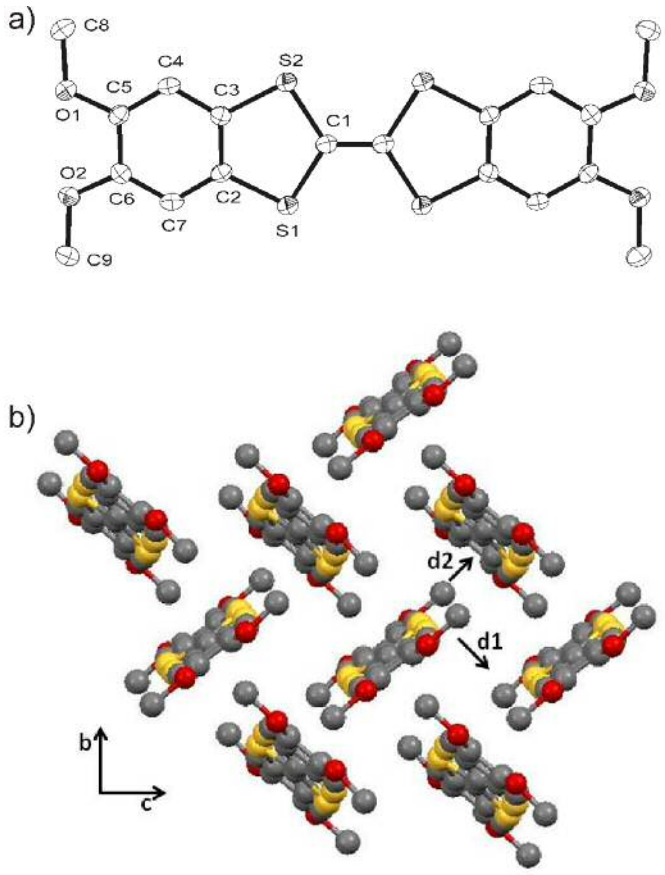

Figure 4. a) ORTEP drawing and atomic numbering scheme of **1**. Ellipsoids are set at 50 % probability, hydrogen atoms have been omitted for clarity. b) Crystal packing of **1**.

Additionally, thin film transistors were also fabricated by thermal evaporation of the organic material in a bottom-gate bottom-contact configuration on Si/SiO_2/OTS substrates (OTS stands for octadecyltrichlorosilane). Gold was used as source and drain electrodes. The first electrical characterisation carried out under darkness and vacuum (P = 50 mbar) was done right after transferring the devices from the evaporation chamber to the microscope probe station. Table 2 shows a summary of the field-effect mobility and threshold voltage of the measured **1-3** thin film transistors. We observe that the V_{TH} extracted for all three compounds gave negative values, which might be an indication of structural disorder at the very edge of the semiconductor/dielectric interface, especially in compounds **2** and **3**. The mobilities extracted in the saturation regime exhibited values around one order of magnitude lower than the single crystals, showing good performance and reproducibility for all the devices. Similar field effect mobilities in the range of 0.8×10^{-3} - 4.2×10^{-3} cm^2/Vs were obtained for compounds **1-3**. Afterwards the samples were measured in air and, in agreement with the calculated and experimentally found HOMO levels, compound **1** with the highest HOMO value showed the lowest stability under ambient conditions. This was reflected in the fact that in the device measurements performed in air a large shift of the threshold voltage of around +14 V was found for devices based on **1**, whereas for the devices employing **2** and **3** as organic semiconductor, a smaller V_{TH} shift of +7 V was observed. Thus, we can affirm that the 2,1,3-chalcogendiazole moiety supports the stabilisation of the materials.

Table 2. Main average device parameters of single crystal (SC) and thin film (TF) OFETs based on **1-3**. μ_{FE} field effect mobility extracted in the saturation regime and V_{TH} threshold voltage extracted in the saturation regime.

	1		**2**		**3**	
	$\mu_{FE}\times10^2$ (cm^2/Vs)	V_{TH} (V)	$\mu_{FE}\times10^2$ (cm^2/Vs)	V_{TH} (V)	$\mu_{FE}\times10^2$ (cm^2/Vs)	V_{TH} (V)
SC	2.0	-1.1	1.4	-4.0	4.0	-0.3
TF	0.4	-11	0.08	-34	0.2	-30

Thin film devices were also prepared on Si/SiO_2 without OTS. In all cases, slightly lower performances and less air stable devices were obtained probably due to a less favourable organic semiconductor/dielectric interface (Figure S6 and S7).

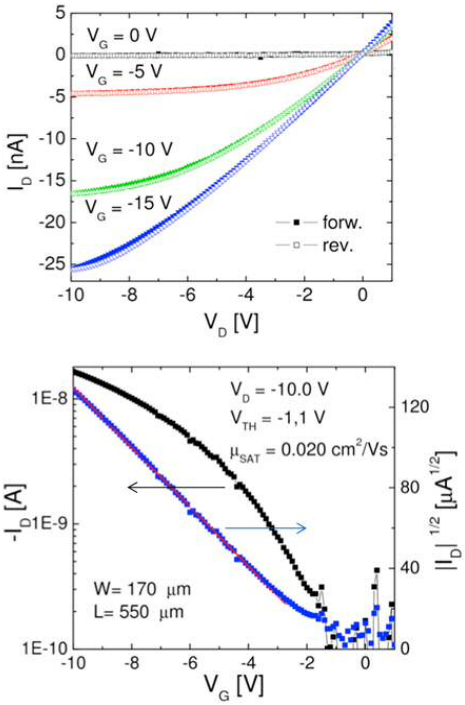

Figure 5. Electrical characterization of a solution grown single crystal of **1**. Output characteristics (top) and corresponding transfer characteristics (bottom).

Both solution grown single crystals and thermally evaporated thin films of **1-3** were characterized by X-ray powder diffraction (XRD). In all cases, the obtained XRD patterns for both device types, *i.e.* solution grown single crystal and thermally evaporated thin film OFETs exhibited the same group of reflections, which is a strong indication that the crystal structure of the measured materials belonged to the same crystalline phase (Figure S8). Furthermore, in the case of **1,** the XRD reflections coincide with the aforementioned resolved single crystal structure of this material (Figure 6). Considering that the observed reflections correspond to the [h00] ones, we can affirm that the measurements in the crystals and thin films of **1** were performed in the *bc* plane, which matches with the directions where short S···S contacts are found and also large transfer integrals have been calculated.

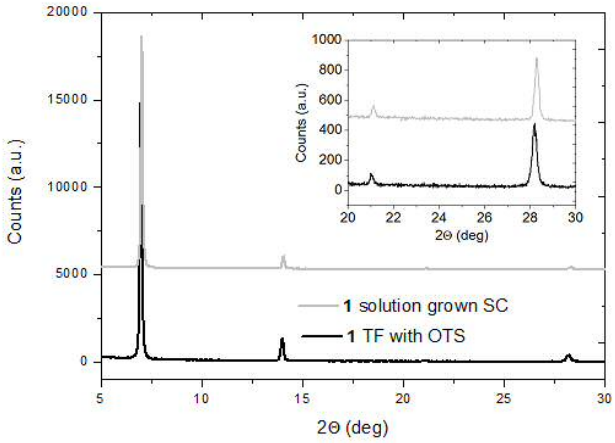

Figure 6. XRD diffraction pattern of solution grown single crystals of **1** and thermally evaporated thin films of **1** on top of a Si/SiO_2/OTS substrate exhibiting the same group of reflections.

For all thermally evaporated thin-films AFM analysis were carried out (Figure S9-S10). Figure 7 shows typical AFM images of **1-3** grown on top of a Si/SiO_2/OTS substrate with micro crystals clearly visible in topography.. The crystallites have an average size of around 0.25 μm^2, but the films were very rough (surface roughness (rms) of 172 nm). On the contrary, the crystallites size in thin films of **2** and **3** were smaller (around 0.1 μm^2) and the thin film roughness was lower (rms of 17.5 and 8.8 nm for **2** and **3**, respectively). We believe that the smaller size of the crystals of **2-3** at the organic semiconductor/dielectric interface might cause the formation of a larger amount of grain boundaries and defects which accounts for the higher negative threshold voltage found for these devices.

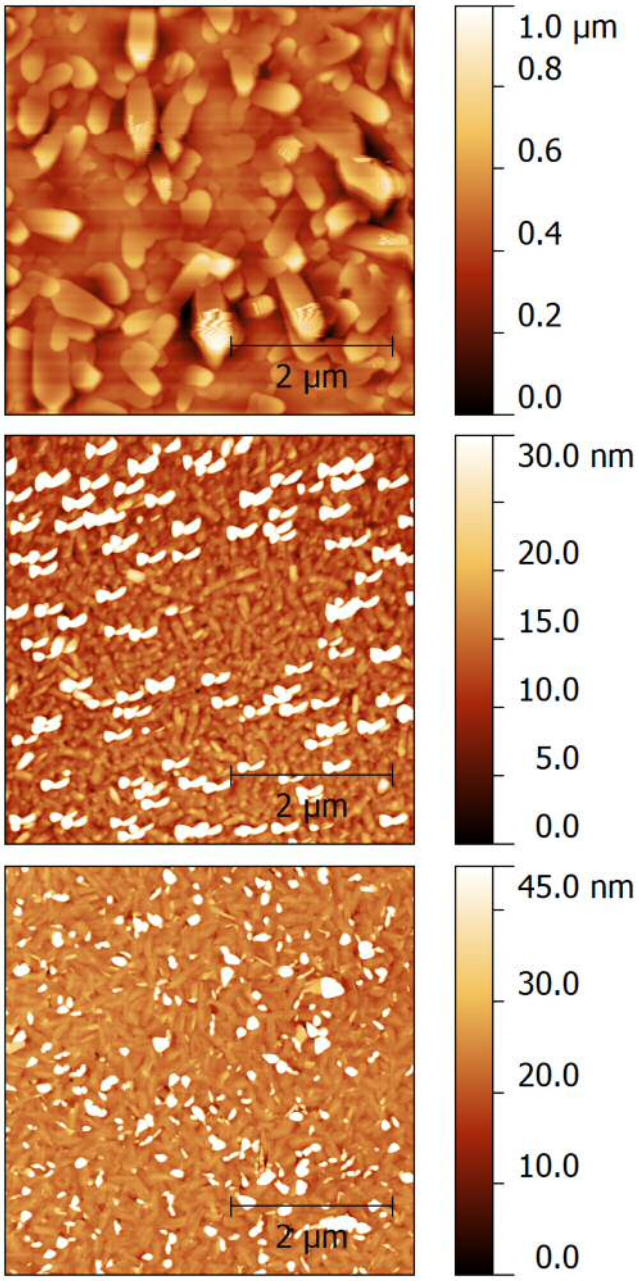

Figure 7. AFM topography images of thermally evaporated thin films of **1-3** (from top to bottom) on top of Si/SiO_2/OTS.

Summary

Rigid electron donor-acceptor conjugates (**2-3**) where a TTF acts as an electron donor and a 2,1,3-benzochalcogendiazole (BCD) as an electron acceptor, have been synthesized and probed with respect to the heteroatom effect on the electronic properties of π-extended DB-TTF derivatives. For a comparative and systematic study, tetramethoxy substituted DB-TTF (**1**) is also described. Their electrochemical, optical absorption, photo-induced intramolecular charge-transfer, and fluorescence characteristics have been presented in detail. Compared to **1**, the electron-withdrawing BCD moiety in **2** and **3** plays a crucial role in tuning the electronic properties. Based on the electrochemistry data and DFT-calculations, one can conclude that the dominant electronic transitions of **2-3** in the visible region show significant intramolecular charge-transfer

character. This result can be accounted for the direct fusion of the BCD unit to the TTF core forming a rigid and planar π-conjugated molecular system. Particularly, our investigation of the chalcogen-property relationship in these compounds reveals a lowering of the HOMO and LUMO energy levels on going from **1** to **3** leading to an increase in the air-stability of the OFETs prepared with these semiconducting materials but without affecting the device mobility. It has been demonstrated that solution-processed single crystal transistors based on **3** exhibit a remarkable hole mobility as well as good ambient stability.

In essence, the present work gives insight into the HOMO stabilisation in π-extended DB-TTF derivatives by virtue of the electron-deficient character of 2,1,3-chalcogendiazole, thus leading to improvement in the ambient stability of the OFET devices. Further work will focus on finely-tuning TTF-BCD topologies via appropriate molecule functionalisation to modulate the intermolecular interactions and morphologies for high-performance OFET devices.

Experimental Section

General: Air and/or water-sensitive reactions were conducted under Ar in dry, freshly distilled solvents. Elemental analyses were performed on an EA 1110 Elemental Analyzer CHN Carlo Erba Instruments. ^{1}H NMR spectra were recorded on a Bruker Avance spectrometer. Chemical shifts are reported in parts per million (ppm) and are referenced to the residual solvent peak (chloroform, ^{1}H = 7.26 ppm, ^{13}C = 77.0 ppm; DSMO, ^{1}H= 2.50 ppm, ^{13}C = 39.6 ppm). Coupling constants (*J*) are given in hertz (Hz) and are quoted to the nearest 0.5 Hz. Peak multiplicities are described in the following way: singlet (s). FT-IR spectra were recorded on a Perkin-Elmer One FT-IR spectrometer. Mass Spectra were recorded with an Auto Spec Q spectrometer for ESI. Cyclic voltammetry (CV) was performed in a three-electrode cell equipped with a Pt-wire as working electrode and counter-electrode, and a silver wire was used as the pseudo-reference electrode. The electrochemical experiments were carried out with a VersaSTAT 3 under dry and an oxygen-free atmosphere in 1,2-dichlorobenzene with $Bu_4N(PF_6)$ (0.1 M) as a support electrolyte, at a scan rate of 100 mV/s and at 150-160°C in order to completely dissolve the compounds. In these conditions, the Fc/Fc^+ redox process occurs at 0.44 V *vs* $Ag_{(s)}$. Optical absorption spectra were recorded on a Perkin Elmer Lambda 900 UV/Vis/NIR spectrometer. Emission spectra were measured on a Perkin Elmer LS50B luminescence spectrometer. Melting point was measured with Büchi B-540 microscope apparatus. *X*-ray diffraction (XRD) measurements for both thermally evaporated thin-films and solution grown crystalline films were performed using a modular X-ray powder diffractometer RIGAKU. Atomic Force Microscopy (AFM) images were taken with a 5500LS SPM system from Agilent Technologies under ambient conditions.

Materials: Unless stated otherwise, all other reagents were purchased from commercial sources and used without additional purification. 4,5-Bis-thiobultylveratrole,[10] [1,3]dithiolo[4,5-*f*]-2,1,3-benzothiadiazole-6-thione (**6**)[12] and [1,3]dithiolo[4,5-*f*]-2,1,3-benzoselenadiazole-6-thione (**7**)[13] were prepared according to literature procedures.

Synthesis of 5,6-dimethoxy-1,3-benzodithiol-2-thione (4): NH_3 (250 mL) was condensed at -78°C in a three-necked flask containing 4,5-bis-thiobultylveratrole (20 g, 63 mmol). Sodium (6.42 g, 279 mmol) was added portion by portion. The reaction mixture became blue. NH_4OH (21g, 600 mmol) was added portion by portion followed by water (1L). The solution was then acidified with concentrated HCl and extracted three times with CH_2Cl_2 (800 ml). Organic phases were collected and washed with water until pH = 7. After evaporation of CH_2Cl_2, the residue was dissolved in water (250 mL) containing KOH (7 g). CS_2 (19 g, 250 mmol) was then added. Afterwards the precipitate was filtered, washed with water and dried in air. Purification by chromatography (Silica gel, CH_2Cl_2) yielded **4** (7.7 g, 50%) as a yellow powder. m.p. 240-241°C; IR (KBr): ν = 3434, 2962, 1590, 1494, 1431, 1371, 1273, 1217, 1074, 1036, 936, 878, 832, 794 cm^{-1}; ^{1}H NMR (300 MHz, $CDCl_3$, 25°C): δ = 6.94 (s, 2H), 3.91 ppm (s, 6H); ^{13}C NMR (300 MHz, $CDCl_3$, 25°C): δ = 221.8, 149.9, 132.6, 104.3, 56.5 ppm; HRMS (ESI): *m/z* calcd for $C_9H_8O_2S_3$: 243.9686; found: 243.9678; Elemental analysis calcd (%) for $C_9H_8O_2S_3$: C 44.24, H 3.30; found: C 44.30, H 3.17.

Synthesis of 5,6-dimethoxy-1,3-benzodithiol-2-one (5): $Hg(OAc)_2$ (1.9 g, 6 mmol) was added to a solution of **4** (488 mg, 2 mmol) in dichloromethane (10 mL). The mixture was stirred at room temperature for 30 min. After filtration and evaporation, **5** (415 mg, 91%) was obtained as a white solid. m.p. 211-212°C; IR (KBr): ν = 3437, 2961, 1649, 1496, 1434, 1368, 1270, 1218, 1040, 942, 866, 837, 794 cm^{-1}; ^{1}H NMR (300 MHz, $CDCl_3$, 25°C): δ = 6.95 (s, 2H), 3.88 ppm (s, 6H); ^{13}C NMR (300 MHz, $CDCl_3$, 25°C): δ = 191.4, 149.4, 123.5, 106.1, 56.5 ppm; HRMS (ESI): *m/z* calcd for $C_9H_8O_3S_2$: 227.9915; found: 227.9905; Elemental analysis calcd (%) for $C_9H_8O_3S_2$: C 47.35, H 3.53; found: C 47.59, H 3.45.

Synthesis of 2-(5,6-dimethoxy-1,3-benzodithiol-2-ylidene)-5,6-dimethoxy-1,3-benzodithiole[22] **(1):** Triethyl phosphite (16 mL) was added to a suspension of **5** (456 mg, 2 mmol) in toluene (8 mL) under Ar. The mixture was refluxed for 3 h. After cooling to room temperature, the resultant precipitate was collected by filtration and washed with MeOH three times to yield **1** (370 mg, 87%) as an orange solid. m.p. decomposed at 340-341°C; IR (KBr): ν = 3437, 2927, 1589, 1568, 1488, 1454, 1435, 1370, 1264, 1209, 1178, 1129, 1041, 854, 832, 787, 771, 691 cm^{-1}; ^{1}H NMR (300 MHz, DMSO-d_6, 25°C): δ = 7.22 (s, 4H), 3.74 ppm (s, 12H); ^{13}C NMR (300 MHz, DMSO-d_6, 25°C): δ =148.0, 125.9, 116.5, 55.9 ppm; MS (ESI): *m/z* calcd for $C_{18}H_{16}O_4S_4$: 423.99; found: 423.99. Elemental analysis calcd (%) for $C_{18}H_{16}O_4S_4$: C 50.92, H 3.80; found: C 51.16, H 3.72.

General procedure for phosphite-mediated cross-coupling reaction: Triethyl phosphite (8 mL) was added to a suspension of [1,3]dithiolo[4,5-*f*]-2,1,3-benzochalcogendiazole-6-thione (1 equivalent) and **5** (2.5 equivalents) in toluene (4 mL) under Ar. The mixture was refluxed for 3 h. After cooling down to room temperature, the resultant precipitate was collected by filtration and washed with MeOH. Purification either by chromatography or by recrystallization affords the analytically pure product.

Synthesis of 6-(5,6-dimethoxy-1,3-benzodithiol-2-ylidene)[1,3]dithiolo[4,5-*f*]-2,1,3-benzothiadiazole[22] **(2):** A reaction starting with **6** (92 mg, 0.4 mmol) and **5** (228 mg, 1 mmol) was performed. The crude product was purified by column chromatography on silica gel eluting initially with CH_2Cl_2 and then THF to afford **2** (60 mg, 36%) as a deep red solid. m.p. 358-359°C; IR (KBr): ν = 3437, 2918, 1631, 1491, 1435, 1371, 1268, 1245, 1214, 1164, 1079, 1046, 839, 811, 780 cm^{-1}; ^{1}H NMR (400 MHz, DMSO-d_6, 80°C): δ = 8.51 (s, 2H), 7.52 (s, 2H), 4.08 ppm (s, 6H), ^{13}C NMR data are unavailable due to its poor solubility; MS (ESI): *m/z* calcd for $C_{16}H_{10}N_2O_2S_5$: 421.93; found: 421.93. Elemental analysis calcd (%) for $C_{16}H_{10}N_2O_2S_5$: C 45.47, H 2.39, N 6.63; found: C 45.09, H 2.18 N 6.64.

Synthesis of 6-(5,6-dimethoxy-1,3-benzodithiol-2-ylidene)[1,3]dithiolo[4,5-*f*]-2,1,3-benzoselenadiazole[22] **(3):** A reaction starting with **7** (116 mg, 0.4 mmol) and **5** (228 mg, 1 mmol) was performed. The resultant precipitate was washed with MeOH and CH_2Cl_2. Then the crude product was recrystallized in toluene to yield **3** (67 mg, 36%) as a deep purple solid. M.p.: 360-361°C; IR (KBr): ν = 3436, 2921, 1589, 1536, 1489, 1436, 1420, 1370, 1344, 1319, 1266, 1212, 1182, 1077, 1045, 1023, 839, 789, 739, 721 cm^{-1}; ^{1}H NMR (400 MHz, DMSO-d_6, 80°C): δ = 8.27 (s, 2H), 7.51 (s, 2H), 4.08 ppm (s, 6H), ^{13}C NMR data are unavailable due to poor solubility; HRMS (ESI): *m/z* calcd for $C_{16}H_{10}N_2O_2S_4Se$: 469.8790; found: 469.8788. Elemental analysis calcd (%) for $C_{16}H_{10}N_2O_2S_4Se$: C 40.93, H 2.15, N 5.97; found: C 41.0, H 2.2, N 5.4.

Crystallography: The single crystal of **1** was mounted with Paratone on a glass needle and used for X-ray structure determination at 173 K. All measurements were made on a Oxford Diffraction SuperNova area-detector diffractometer[23] using mirror optics monochromated MoK_α radiation (λ = 0.71073 Å). The unit cell constants and an orientation matrix for data collection were obtained from a least-squares refinement of the setting angles of 2975 reflections in the range $2.41° < \theta < 25.63°$. A total of 1152 frames were collected using ω scans, 60 seconds exposure time and a rotation angle of 1.0° per frame, and a crystal-detector distance of 66.2 mm. Data reduction was performed using the CrysAlisPro[23] program. The intensities were corrected for Lorentz and polarization effects, and an absorption correction based on the multi-scan method using SCALE3 ABSPACK in CrysAlisPro[23] was applied. The structure was solved by direct methods using SIR97,[24] which revealed the positions of all non-hydrogen atoms. The non-hydrogen atoms were refined anisotropically. All H-atoms were placed in geometrically calculated positions and refined using a riding model where each H-atom was assigned a fixed isotropic displacement parameter with a value equal to 1.2 Ueq of its parent atom atom (1.5 Ueq for the methyl group). Refinement of the structure was carried out on F^2 using full-matrix least-squares procedures, which minimized the function $\Sigma w(F_o^2 - F_c^2)_2$. The weighting scheme was based on counting statistics and included a factor to downweight the intense reflections. All calculations were performed using the SHELXL-97[25] program. Crystallographic data, CCDC 991425 (**1**) can be obtained free of charge from the Cambridge Crystallographic Data Centre via www.ccdc.cam.ac.uk/data_request/cif.

Preparation of solution processed single crystal OFETs: Bare Si/SiO_2 wafer pieces were used as a substrate (purchased at Si-Mat). Highly *n*-doped silicon was used as a common gate electrode. The thickness of the dielectric layer was about 50 nm. Compounds **1** and **2** were dissolved in 1,2-dichlorobenzene with a concentration of c = 1/2 mg/ml at T = 100°C. Silicon substrates were stored within an oven at T = 100°C before drop-casting the hot solution and covered with a Petri dish to slow down the evaporation process. After the solvent evaporated completely the samples were cooled

down slowly to room temperature to prevent stress in the crystals. Single crystals of compound **3** were grown at ambient temperature from 1,2-dichlorobenzene with a concentration of c = 1/2 mg/ml. Source and drain electrodes were fabricated with graphite paste (Dotite XC-12) [26] for **1** and **2**. After drying the graphite paste for 1 h at ambient conditions, the electrical characterization was carried out with a Keithley 2612A Source Meter under ambient conditions and darkness. For **3** prefabricated Cr/Au electrodes were used as source and drain. Channel length and width of all devices were measured with an Olympus BX51 optical microscope.

Preparation of thermally evaporated thin film OFETs: Si/SiO_2 wafer pieces with ITO/Au as source and drain inter-digitated electrodes (W = 10 mm, L = 20, 10, 5 µm) in a bottom-gate bottom-contact geometry (purchased at Fraunhofer, IPMS) were used as a substrate. Highly n-doped silicon was used as a common gate electrode. The thickness of the dielectric layer was about 230 nm. TTF derivatives **1**-**3** were thermally evaporated at T = 170-200°C, 180-200°C and 190-230°C, respectively. The pressure within the vacuum chamber was about $p = 2\times10^{-6}$ mbar and the evaporations were carried out employing a rate of about 0.5 Å/s. Two different device-types were prepared, where in the first case the organic material was directly evaporated on bare SiO_2, while in the second case an OTS (octadecyltrichlorosilane) monolayer was applied to the SiO_2 before the deposition of the active material. After the deposition of the active material the samples were transferred to the electrical characterization system as quickly as possible (*i.e.* less than 1 minute) to reduce exposure to ambient conditions. The measurement system was equipped with micromanipulators for easy connection in a vacuum chamber (p ~ 50 mbar). The electrical characterization was done with an (Hewlett-Packard semiconductor parameter analyzer 4156A) under darkness. With the aim to obtain information regarding ambient stability of the evaporated films, the devices were measured under environmental conditions and darkness (RH = 40-60 %) with a Keithley 2612A Source Meter and home made routines for device control. Field-effect mobility and the threshold voltage were extracted in the saturation regime using relation: [27]

$$\mu_{SAT} = \frac{2L}{WC_i}\left(\frac{\partial\sqrt{I_{SD,SAT}}}{\partial V_{SG}}\right)^2$$

Theoretical calculations of the HOMO-LUMO and transfer integrals: In order to calculate the electronic energy levels, density functional theory (DFT) calculations using the B3LYP functional and a 6-311G+(d, p) basis set as implemented in the Gaussian 09 code[17] were used. The results were obtained by single point energy calculations using the structure obtained by single crystal X-ray diffraction in the case of **1**, and by optimizing the structure in the cases of **2** and **3**. TTF derivatives relax to a bent boat-like conformation in free space whereas they exhibit a planar conformation in molecular crystals. In order to approximate this structural tendency, we restricted the atoms to lie in a single plane in the structural optimisations of molecules **2** and **3**.[28] We note that this minor structural restriction only destabilises the molecules by 3-4 kJ/mol but improves the agreement with experiment with respect to the HOMO and energy gap by 0.1-0.15 eV.

Acknowledgements

Financial support for this research by the Swiss National Science Foundation (Grant No. 200021-147143), ERC StG 2012-306826 e-GAMES, the Networking Research Center on Bioengineering, Biomaterials and Nanomedicine (CIBER-BBN), the DGI (Spain) with project POMAS CTQ2010-19501/BQU, TEC2011-27859-C02-01, and MAT2012-30924 as well as by the National Natural Science Foundation of China (No. 21175077) and the Taishan Scholar Program of Shandong Province, is gratefully acknowledged.

[1] a) *Organic Field-Effect Transistors*, (Eds: Z. Bao, J. Locklin), CRC Press, New York, **2007**; b) M. Mas-Torrent, C. Rovira, *Chem. Soc. Rev.* **2008**, *37*, 827; c) M. Mas-Torrent, C. Rovira, *Chem. Rev.* **2011**, *111*, 4833; d) A. Fachhetti, *Chem. Mater.* **2011**, *23*, 733.

[2] a) M. Mas-Torrent, M. Durkut, P. Hadley, X. Ribas, C. Rovira, *J. Am. Chem. Soc.* **2004**, *126*, 984; b) V. C. Sundar, J. Zaumseil, V. Podzorov, E. Menard, R. L. Willett, T. Someya, M. E. Gershenson, J. A. Rogers, *Science* **2004**, *303*, 1644; c) M. Mas-Torrent, C. Rovira, *J. Mater. Chem.* **2006**, *16*, 433; d) R. Pfattner, E. Pavlica, M. Jaggi, S.-X. Liu, S. Decurtins, G. Bratina, J. Veciana, M. Mas-Torrent, C. Rovira, *J. Mater. Chem. C*, **2013**, *1*, 3985; e) J. Takeya, M. Yamaguchi, Y. Tominari, R. Hirahata, Y. Nakazawa, T. Nishikawa, T. Kawase, T. Shimoda, S. Ogawa, *Appl. Phys. Lett.* **2007**, *90*, 102120; f) Y. Takahashi, T. Hasegawa, S. Horiuchi, R. Kumai, Y. Tokura, G. Saito, *Chem. Mater.* **2007**, *19*, 6382; g) X. K. Gao, Y. Wang, X. D. Yang, Y. Q. Liu, W. F. Qiu, W. P. Wu, H. J. Zhang, T. Qi, Y. Liu, K. Lu, C. Y. Du, Z. G. Shuai, G. Yu, D. B. Zhu, *Adv. Mater.* **2007**, *19*, 3037.

[3] a) M. Mas-Torrent, P. Hadley, S. T. Bromley, N. Crivillers, C. Rovira, *Appl. Phys. Lett.* **2005**, *86*, 012110; b) Naraso, J. Nishida, S. Ando, J. Yamaguchi, K. Itaka, H. Koinuma, H. Tada, S. Tokio, Y. Yamashita, *J. Am. Chem. Soc.* **2005**, *127*, 10142; c) K. Shibata, K. Ishikawa, H. Takezoe, H. Wada, T. Mori, *Appl. Phys. Lett.* **2008**, *92*, 023305; d) T. Yamada, T. Hasegawa, M. Hiraoka, H. Matsui, Y. Tokura, G. Saito, *Appl. Phys. Lett.* **2008**, *92*, 233306; e) M. Leufgen, O. Rost, C. Gould, G. Schmidt, J. Geurts, L. W. Molenkamp, N. S. Oxtoby, M. Mas-Torrent, N. Crivillers, J. Veciana, C. Rovira, *Org. Electron.* **2008**, *9*, 1101; f) A. Brillante, I. Bilotti, R. G. Della Valle, E. Venuti, S. Milita, C. Dionigi, F. Borgatti, A. N. Lazar, F. Biscarini, M. Mas-Torrent, N. S. Oxtoby, N. Crivillers, J. Veciana, C. Rovira, *CrystEngComm*. **2008**, *10*, 1899.

[4] a) J. Inoue, M. Kanno, M. Ashizawa, C. Seo, A. Tanioka, T. Mori, *Chem. Lett.* **2010**, 538; b) J. Nagakubo, M. Ashizawa, T. Kawamoto, A. Tanioka, T. Mori, *Phys. Chem. Chem. Phys.* **2011**, *13*, 14370; c) T. Yoshino, K. Shibata, H. Wada, Y. Bando, K. Ishikawa, H. Takezoe, T. Mori, *Chem. Lett.* **2009**, *38*, 200; d) K. Omata, M. Mamada, J.-i. Nishida, S. Tokito, Y. Yamashita, *Bull. Chem. Soc. Jpn.* **2010**, *83*, 575; e) M. Mas-Torrent, P. Hadley, N. Crivillers, J. Veciana, C. Rovira, *ChemPhysChem* **2006**, *7*, 86; f) J. Casado, M. Z. Zgierski, D. M. C. Ruiz, N. J. T. Lopez, M. Mas-Torrent, C. Rovira, *J. Phys. Chem. C* **2007**, *111*, 10110;. g) F. Otón, R. Pfattner, E. Pavlica, Y. Olivier, E. Moreno, J. Puigdollers, G. Bratina, J. Cornil, X. Fontrodona, M. Mas-Torrent, J. Veciana and C. Rovira, *Chem. Mater.* **2011**, *23*, 851; h) F. Otón, R. Pfattner, N. S. Oxtoby, M. Mas-Torrent, K. Wurst, X. Fontrodona, Y. Olivier, J. Cornil, J. Veciana, C. Rovira, *J. Org. Chem*. **2011**, *76*, 154; i) F. Otón, R. Pfattner, E. Pavlica, Y. Olivier, G. Bratina, J. Cornil, J.Puigdollers, R. Alcubilla, X. Fontrodona, M. Mas-Torrent, J. Veciana, C. Rovira, *CrystEngComm*. **2011**, *13*, 6597; j) F. Otón, V. Lloveras, M. Mas-Torrent, J. Vidal-Gancedo, J. Veciana, C. Rovira, *Angew. Chem. Int. Ed*. **2011**, *50*, 10902.

[5] a) Y. Wu, W. Zhu, *Chem. Soc. Rev.* **2013**, *42*, 2039; b) C. R. Belton, A. L. Kanibolotsky, J. Kirkpatrick, C. Orofino, S. E. T. Elmasly, P. N. Stavrinou, P. J. Skabara, D. D. C. Bradley, *Adv. Funct. Mater.* **2013**, *23*, 2792; c) L. V. Brownell, K. Jang, K. A. Robins, I. C. Tran, C. Heske, D.-C. Lee, *Phys. Chem. Chem. Phys.* **2013**, *15*, 5967; d) M. Scarongella, A. Laktionov, U. Röhtlisberger, N. Banerji, *J. Mater. Chem. C* **2013**, *1*, 2308; e) G. Yang , C.-A. Di, G. Zhang, J. Zhang, J. Xiang, D. Zhang, D. Zhu, *Adv. Funct. Mater.* **2013**, *23*, 1671.

[6] a) F. Pop, A. Amacher, N. Avarvari, J. Ding, L. M. L. Daku, A. Hauser, M. Koch, J. Hauser, S.-X. Liu, S. Decurtins, *Chem. Eur. J.* **2013**, *19*, 2504; b) A. Amacher, H. Luo, Z. Liu, M. Bircher, M. Cascella, J. Hauser, S. Decurtins, D. Zhang, S.-X. Liu, *RSC Adv.* **2014**, *4*, 2873.

[7] a) X. Guo, S. Reddy Puniredd, M. Baumgarten, W. Pisula, K Müllen, *J. Am. Chem. Soc.* **2012**, *134*, 8404; b) M. Zhang, H. N. Tsao, W. Pisula, C. Yang, A. K. Mishra, K. Müllen, *J. Am. Chem. Soc.* **2007**, *129*, 3472; c) J. Hou, H.-Y. Chen, S. Zhang, G. Li, Y. Yang, *J. Am. Chem. Soc.* **2008**, *130*, 16144; d) H. N. Tsao, D. M. Cho, I. Park, M. R. Hansen, A. Mavrinskiy, D. Y. Yoon, R. Graf, W. Pisula, H. W. Spiess, K. Müllen, *J. Am. Chem. Soc.* **2011**, *133*, 2605.

[8] a) K. Takimiya, S. Shinamura , I. Osaka , E. Eigo Miyazak, *Adv. Mater.* **2011**, *23*, 4347; b) K. Xiao, Y. Liu, T. Qi, W. Zhang, F. Wang, J. Gao, W. Qiu, Y. Ma, G. Cui, S. Chen, X. Zhan,G Yu, J. Qin, W. Hu, D. Zhu, *J. Am. Chem. Soc.* **2005**, *127*, 13285; c) I.McCulloch, C. Bailey, M. Giles, M. Heeney, I. Love, M. Shkunov, D. Sparrowe, S.Tierney, *Chem. Mater.* **2005**, *17*, 1381.

[9] a) Y. Li, S. P. Singh, P. Sonar, *Adv. Mater.* **2010**, *43*, 4862; b) J. Fan, J. D. Yuen, M. Wang, J. Seifter, J.-H. Seo, A. R. Mohebbi, D. Zakhidov, A. Heeger, F. Wudl, *Adv. Mater.* **2012**, *24*, 2186.

[10] D. Coucouvanis, A. R. Paital, Q. Zhang, N. Lehnert, R. Ahlrichs, K. Fink, D. Fenske, A. K. Powell, Y. Lan, *Inorg. Chem.* **2009**, *48*, 8830.

[11] a) R. Adams, A. Ferretti, *J. Am. Chem. Soc.* **1959**, *81*, 4927; b) R. Adams, A. Ferretti, *Org. Synth.* **1962**, *42*, 54.

[12] a) H.-P. Jia, J. Ding, Y.-F. Ran, S.-X. Liu, C. Blum, I. Petkova, A. Hauser, S. Decurtins, *Chem. Asian J.* **2011**, *6*, 3312; b) Y. Geng, R. Pfattner, A. Campos, J. Hauser, V. Laukhin, J. Puigdollers, J. Veciana, M. Mas-Torrent, C. Rovira, S. Decurtins, S.-X. Liu, *Chem. Eur. J.* **2014**, *20*, 7136.

[13] W. Wang, N. Zhao, Y. Geng, S.-B. Cui, J. Hauser, S. Decurtins, S.-X. Liu, *RSC Adv.* **2014**, DOI: 10.1039/C4RA06455K.

[14] J. Pomrnerehne, H. Vestweber, W. Gun, R. E: Muhrt, H. Bassler, M.Porsch, J. Daub, *Adv. Mater.* **1995**, *7*, 551.

[15] D. Mi, H.-U. Kim, J.-H. Kim, F. Xu, S.-H. Jin, D.-H. Hwang, *Synth. Met*. **2012**, *162*, 483.

[16] P. J. Stephens, F. J. Devlin, C. F. Chabalowski, M. J. Frisch, *J. Phys. Chem.* **1994**, *98*, 11623.

[17] *Gaussian 09*, M. J. Frisch, G. W. Trucks, H. B. Schlegel, G. E. Scuseria, M. A. Robb, J. R. Cheeseman, G. Scalmani, V. Barone, B. Mennucci, G. A. Petersson, H. Nakatsuji, M. Caricato, X. Li, H. P. Hratchian, A. F. Izmaylov, J. Bloino, G. Zheng, J. L. Sonnenberg, M. Hada, M. Ehara, K. Toyota, R. Fukuda, J. Hasegawa, M. Ishida, T. Nakajima, Y. Honda, O. Kitao, H. Nakai, T. Vreven, J. A. Montgomery, Jr., J. E. Peralta, F. Ogliaro, M. Bearpark, J. J. Heyd, E. Brothers, K. N. Kudin, V. N. Staroverov, R. Kobayashi, J. Normand, K. Raghavachari, A. Rendell, J. C. Burant, S. S. Iyengar, J. Tomasi, M. Cossi, N. Rega, J. M. Millam, M. Klene, J. E. Knox, J. B. Cross, V. Bakken, C. Adamo, J.

Jaramillo, R. Gomperts, R. E. Stratmann, O. Yazyev, A. J. Austin, R. Cammi, C. Pomelli, J. W. Ochterski, R. L. Martin, K. Morokuma, V. G. Zakrzewski, G. A. Voth, P. Salvador, J. J. Dannenberg, S. Dapprich, A. D. Daniels, Ö. Farkas, J. B. Foresman, J. V. Ortiz, J. Cioslowski, and D. J. Fox, Gaussian, Inc., Wallingford CT, **2009**.

[18] J. Huang, M. Kertesz, *J. Phys. Chem*. **2005**, *122*, 234707.

[19] J. P. Perdew, J. A. Chevary, S. H. Vosko, K. A. Jackson, M. R. Pederson, D. J. Singh, C. Fiolhais, *Phys. Rev. B* **1992**, *46*, 6671.

[20] C. Moreno, R. Pfattner, M. Mas-Torrent, J. Puigdollers, S. T. Bromley, C. Rovira, J. Veciana, R. Alcubilla, *J. Mater. Chem.* **2012**, *22*, 345.

[21] a) X. Gao, W. Wu, Y. Liu, W. Qiu, X. Sun, G. Yu, D. Zhu, *Chem. Commun.* **2006**, 2750; b) I. Doi, E. Miyazaki, K. Takimiya,Y. Kunugi, *Chem. Mater.* **2007**, *19*, 5230.

[22] U. Bünzli-Trepp, in *Systematic Nomenclature of Organic, Organometallic and Coordination Chemistry,* EPFL, Lausanne, **2007**.

[23] *Oxford Diffraction CrysAlisPro (Version 1.171.34.36)*, Oxford Diffraction Ltd., Yarnton, Oxfordshire, UK, **2010**.

[24] A. Altomare, M. C. Burla, M. Camalli, G. Cascarano, C. Giacovazzo, A. Guagliardi, A. G. G. Moliterni, G. Polidori, R. Spagna, *J. Appl. Crystallogr.* **1999**, *32*, 115.

[25] G. M. Sheldrick, *Acta Cryst.* **2008**, *A64*, 112.

[26] R. Pfattner, M. Mas-Torrent, I. Bilotti, A. Brillante, S. Milita, F. Liscio, F. Biscarini, T. Marszalek, J. Ulanski, A. Nosal, M. Gazicki-Lipman, M. Leufgen, G. Schmidt, L. W. Molenkamp, V. Laukhin, J. Veciana, C. Rovira, *Adv. Mater.* **2010**, *22*, 4198.

[27] G. Horowitz, R. Hajlaoui, H. Bouchriha, R. Bourguiga, M. Hajlaoui, *Adv. Mater.* **1998**, *10*, 923.

[28] S. T. Bromley, M. Mas-Torrent, P. Hadley, C. Rovira, *J. Am. Chem. Soc.* **2004**, *126*, 6544.